Flexible Transfer Converters Enabling Autonomous Control and Power Dispatch of Microgrids

Ronghui An, *Student Member, IEEE*, Jinjun Liu, *Fellow, IEEE*, Zeng Liu, *Member, IEEE*, and Zhaoqi Song

***Abstract*—For grid-connected or interconnected microgrids, the transition to an autonomous and decentralized architecture was hampered by two perplexing issues: how to guarantee voltage-supporting capacity, while fully and controllably utilizing local power generation, and how to switch between islanded and grid-connected modes flexibly and seamlessly. Through a combination of benefits of interlinking converters and switches, the flexible transfer converters (FTCs), positioned at the interfaces between the utility grid and microgrids, are offered as a solution in this article. The basic concepts and classifications of the FTC are first presented, and a general-purpose FTC and a universal control strategy for distributed generations are then proposed as an example, which contribute to appropriate power dispatch and flexible mode transfer in a communication-free design, leading to a fully autonomous microgrid. Simple and economic operation rules, as well as high interoperability with existing assets, makes this solution promising for distributed microgrid applications. Further, generalized small-signal models of the target system are derived for stability analysis and parameter design. Finally, comprehensive case studies in simulations and experiments are provided to validate its effectiveness.**

***Index Terms*—Autonomous control, flexible transfer converter (FTC), microgrid, presynchronization, universal control.**

I. Introduction

With the progressive integration of distributed renewable energy sources (RESs) into the power system, the microgrid, a localized group of sources and loads with the capability to operate either as a grid-connected or as an islanded system, was regarded as a key component of future power system and has become one of research focuses in the last decades. A real distributed microgrid may comprise numerous distributed generations (DGs) and dispersed loads, which are usually located far from each other and connected to the microgrid bus through different wires or even a mesh structure. In this situation, a peer-to-peer decentralized control strategy that relies only on local information naturally outperforms the centralized and distributed ones in terms of reliability and cost, as it is unaffected by any single point of failure at the DG or communication link [1], [2]. Besides, the control rules should be simple and entirely scalable, and accurate and real-time knowledge of the system topology or state, as well as complex central computations, should be avoided. Then, these desired attributes can generally characterize the basic blueprint of an autonomous microgrid.

In islanded mode, DGs should work together to achieve bus voltage regulation and supply local loads in the microgrid according to their capacities, whereas in grid-connected mode, they switch to power sources to meet their own financial objectives, as the bus voltage is supported by the utility grid instead. Then, a switch of control structure or power reference may be necessary due to this discrepancy in the control target [3]. However, real-time operating mode awareness relies on communication with the grid interface [4]–[7] or islanding detection [8], [9], and the islanding detection methods suffer from low reliability and time delays despite the fact that they eliminate the need for communication. Alternative solutions are based on a universal controller for both modes [10]–[12]. Unfortunately, in these methods, there is always a tradeoff between the power tracking performance in the grid-connected mode and the voltage quality in the islanded mode.

Aside from the control method, another significant duty for DGs in the transition from islanded to grid-connected mode is to presynchronize the microgrid with the utility grid before reconnection, which can be divided into two types: passive and active synchronizations [3]. The passive synchronization, on the one hand, assumes that the microgrid and utility grid have similar voltage magnitudes but slightly different frequencies, and that the connection occurs when their phases overlap. Active synchronization, on the other hand, means that all DGs in voltage control mode must participate in the synchronization process and adjust their output voltages according to the grid-side measurements simultaneously [5], [7], [10], [13], [14]. As a result, a quick and seamless connection is achieved, but high-bandwidth communication links are essential to deliver compensation signals to each DG.

These two perplexing issues cannot be effectively addressed without a link to communicate grid-side information among DGs, which violates the communication-free feature and has become a bottleneck to enabling an autonomous microgrid. This is partly due to the fact that conventional grid interfaces usually employ mechanical or static switches to transfer the microgrid between islanded and grid-connected modes. Their

Manuscript received 8 March 2022; revised 2 May 2022 and 30 May 2022; accepted 2 June 2022. Date of publication 7 June 2022; date of current version 26 July 2022. This work was supported in part by the National Natural Science Foundation of China under Grant 52077174. An earlier version of this paper was presented in part at the 37th Annual IEEE Applied Power Electronics Conference and Exposition [DOI: 10.1109/APEC43599.2022.9773607]. Recommended for publication by Associate Editor A. Davoudi. *(Corresponding authors: Jinjun Liu; Zeng Liu.)*

The authors are with the State Key Lab of Electrical Insulation and Power Equipment, School of Electrical Engineering, Xi'an Jiaotong University, Xi'an 710049, China (e-mail: an_ronghui@163.com; jjliu@mail.xjtu.edu.cn; zengliu@mail.xjtu.edu.cn; zhaoqisong_xjtu@outlook.com).

Color versions of one or more figures in this article are available at https://doi.org/10.1109/TPEL.2022.3180562.

Digital Object Identifier 10.1109/TPEL.2022.3180562

TABLE I
COMPARISON OF GRID INTERFACES

	Switches	Power Electronic Converters
Efficiency	High	Low
Cost	Low	High
Reliability	High	Low
Current Carrying Capability	High	Low
PFC	×	√
Active Reconnection	×	√
Auxiliary Services	×	√

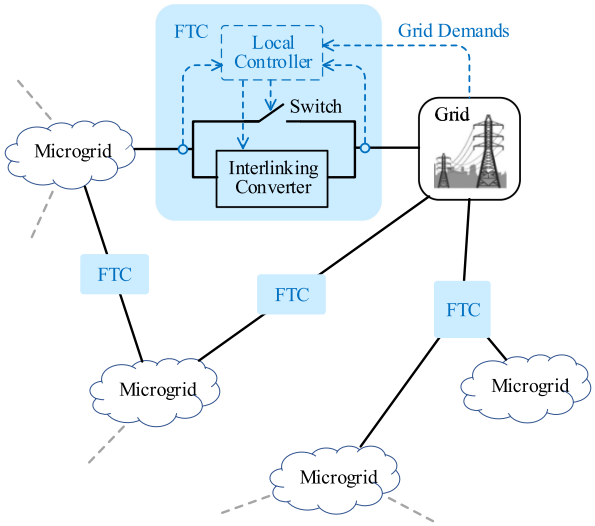

Fig. 1. FTCs as interfaces between the utility grid and microgrids.

passive nature limits their influence on power dispatch and bus voltage control, although they have obvious strengths in cost and efficiency [15]. By contrast, power-electronic-converter-based interfaces, i.e., interlinking converters (ICs), have the potential to manage power flow and actively participate in the auxiliary services even when the connected networks are not synchronized, and thus are thought to be the key to integrating microgrids into the power system [16]. The IC interfaces are more versatile than switches, but they are also more expensive, inefficient, and unreliable, and power dispatch at the interface is always restricted by its capacity. Table I tabulates a simple comparison between these two kinds of grid interfaces.

Therefore, in this work, the flexible transfer converter (FTC) is provided as a solution for enabling autonomous control and power dispatch of microgrids. The FTC is an auxiliary device made up of a topology-specific IC integrated with a bypass switch, which is installed at the interface between the utility grid and microgrid, or between microgrids, as shown in Fig. 1. It combines the benefits of IC and switch through reasonable coordination of them, i.e., it can achieve a fast and soft reconnection, dispatch power through the IC in response to grid demands or based on local measurements, autosynchronize both sides and smoothly transfer to the bypass switch for long-term connection or IC capacity shortage. As a result, the target systems are most of the time connected in a reliable and high-efficiency manner, while the FTC can still perform all the functions when necessary. As the switch shares a large portion of pressures on the IC, the IC's capacity can be reduced, and its service life can be greatly extended, resulting in a lower cost per unit time compared with pure IC interfaces.

The FTC is a broad concept that encompasses a variety of possible topologies and the corresponding control strategies, and because of its various operating modes, it necessitates a higher level of coordination with the DGs. Following is a summary of some related research. Autonomous power flow control (PFC) methods of ICs for hybrid ac/dc microgrids were discussed in [17]–[19], where the normalized bus voltage or frequency was used to identify the output power condition on each side, however they would lose accuracy in the cases of distributed microgrids, for the voltage drops on transmission lines could not be ignored. In contrast, in ac microgrids, the fundamental frequency is a global variable that can be used to coordinate the IC and DGs, allowing autonomous control to be achieved [16], [20]–[22]. In these literatures, the IC and DGs are somehow merged as a single entity, and the IC controls its voltage or output power to reach a certain objective based on the predefined DG characteristics. Since the DGs were controlled as droop or inverse-droop sources, they cannot perform well in both islanded and grid-connected modes without the IC. Further, in [23] and [24], the soft open points and similar devices were employed to energize an isolated area and resynchronize it with its original feeder. In [5], [10], and [25]–[27], a special DG was used to presynchronize the microgrid with the grid in a master–slave manner, but the other DGs relied too heavily on it in islanded mode [25], [26], and additional communications were required to avoid it overloading [5], [27]. In [28] and [29], special devices injected certain power to affect the power balance, and then, the synchronous generator (SG) or SG-based microgrid was accelerated to synchronize with the utility grid. However, communicating with multiple DGs to switch control modes is more difficult than with an SG.

In a nutshell, while the solutions in previous works could perform some of the functions of an FTC, they have not fully established the basic framework of an autonomous microgrid involving multiple prosumers, for the IC appears to play too much of a leading role in the entire system and the DGs' responsibilities are weakened. Therefore, in this article, the DGs are designed to support the local bus cooperatively and achieve their own financial targets through a universal control strategy in both modes, and the FTC is employed to provide auxiliary services and help deal with extreme situations.

This article focuses on how to develop a more flexible grid interface for ac microgrids, i.e., the FTC, as well as how to enable an autonomous microgrid with it, how to appropriately coordinate it with the utility grid and DGs in the microgrid(s), and how to coordinate the two power flow paths in it. The primary contributions are summarized as follows.

1) Basic concepts, operating modes, and classifications of the FTC are introduced. Compared with the conventional interfaces, the FTC enhances the flexibility, reliability, and efficiency of target system, while also extending the IC's service life to its maximum extent and making IC maintenance easier.

2) A general-purpose FTC and its basic control methods are presented as an example, which can appropriately control the power dispatch, and flexibly switch the microgrid between different modes without communications with DGs.
3) A universal control strategy for DGs in the connected microgrid is proposed, which can achieve good performance in both modes and coordinate with the FTC in a completely decentralized manner.
4) A comprehensive solution, which provides all necessary characteristics of an autonomous microgrid, is obtained based on reasonable coordination of the FTC and DGs.
5) Generalized small-signal models of the target system are derived for stability analysis and parameter design. They are also applicable to other kinds of FTCs, as well as laying the groundwork for further enhancement of control methods.

The rest of this article is organized as follows. Section II introduces the basic operating modes and classifications of FTC, followed by Sections III and IV, which detail the control methods for the general-purpose FTC and DGs, respectively. In Section V, the coordination of FTC and DGs and its salient features are discussed. In Section VI, the generalized models of FTC-connected system are derived and analyzed. Simulation and experimental verifications are presented in Section VII. Finally, Section VIII concludes this article.

II. Operating Modes and Classifications

In an autonomous microgrid, numerous DGs are always pursuing their own financial objectives, but for redundancy and reliability reasons, the majority of them, especially those with larger capacities, must work together to support the bus voltage, while the FTC serves as a microgrid representative, coordinating with the grid and providing auxiliary services for both sides.

A. Basic Operating Modes of FTC

Three basic operating modes of the FTC, their transferring paths, and the corresponding functions that could be provided are illustrated in Fig. 2. As shown in Fig. 2, the grid-connected mode can be classified into synchronous connection mode (SCM) and asynchronous connection mode (ACM) according to whether the grid is connected through the switch or the IC. In the ACM, the switch remains open, and the IC controls power dispatch in response to the grid demands or based on local measurements. The detailed control logics of these two modes will be discussed in the next section. When the utility grid no longer requires a specific power injection and allows a long-term free connection, or the IC capacity is not enough to complete its control targets, the FTC will control the power flow to autosynchronize with the grid and seamlessly transfer to the SCM to reduce transmission losses. Meanwhile, the IC can be shutdown to extend its service life or reassigned to provide other auxiliary services, while the grid demands and microgrid conditions are continuously monitored. When any type of islanding occurs, the FTC immediately stops power dispatching and transfers to the islanded mode, leaving the DGs to supply local loads; however, during the reconnection process, the FTC must start from the ACM first. Moreover, auxiliary services, such as reactive power regulation, harmonic and unbalance compensation, fault protection, and resonance damping, can all be provided by the FTC in any mode [16]. It is worth noting that the FTCs that connect two microgrids have the same operating modes, however, the SCM is only activated when one side experiences a constant energy shortage.

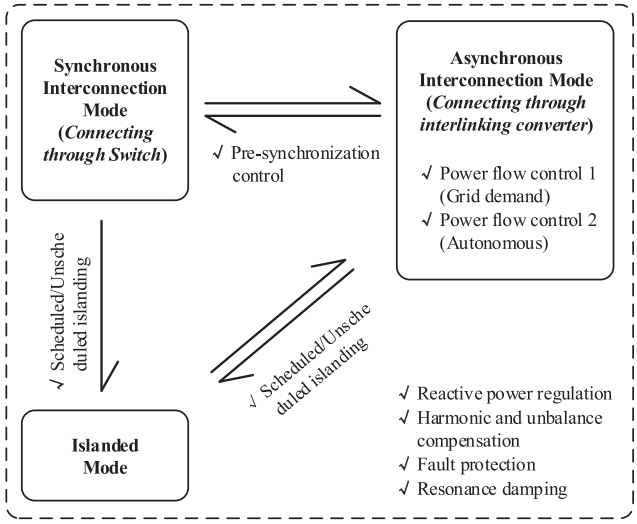

Fig. 2. Operating modes, transferring paths, and functions of the FTC.

As a result, two power flow paths are available at the grid interface: one is wide, efficient, but unforced, whereas the other is relatively narrow, lossy, but controllable. The FTC will switch between them based on the circumstances to form a more flexible and cost-effective interface. A detailed example will be presented in Section V.

B. Classifications of FTC

The FTC is a broad concept that encompasses a variety of possible topologies and the corresponding control strategies, and each must be designed adaptively based on the features of the connected microgrids. Therefore, microgrids are roughly classified into three types according to their operating modes first: normally islanded, normally connected, and ordinary, with their application scenarios, demands, and available FTCs listed in Table II. Due to the restricted number of pages, only the general-purpose FTC, which can handle more uncertainties, will be discussed in detail in this article.

The general-purpose FTC must deal with highly uncertain local generation and multiple individual prosumers, as well as connect or disconnect from the grid flexibly and seamlessly, making the connected microgrid a controllable load. Therefore, when selecting a proper IC topology, it is critical to consider not only the functions, but also cost and efficiency. According to the connection scheme of IC and the connected system(s), the possible topologies of the FTC are classified into shunt, series, and cascaded types, and the cascaded type is further classified into direct ac–ac, indirect ac–ac, and fractional-rated converters, with their schematics, examples, and key properties illustrated

TABLE II
CLASSIFICATION OF MICROGRIDS AND FTCS

Microgrid Type	Application Scenarios	FTC		
		Demand for Efficiency	Demand for Flexibility	Available Type(s)
Normally islanded	✓ Sufficient local generation and energy storage to supply local loads; ✓ Connect to utility grid only when energy shortage occurs in microgrid	Low	Low	Normally islanded FTC (or general-purpose FTC)
Normally connected	✓ Insufficient generation to steadily supply local loads, or a large surplus of generation can be fed into utility grid; ✓ Island only when utility faults or contingencies happen	High	Low	Normally connected FTC (or general-purpose FTC)
Ordinary	✓ Highly uncertain local generation or multiple individual prosumers; ✓ Need to transfer between islanded and grid-connected modes flexibly and seamlessly	Relatively high	High	General-purpose FTC

TABLE III
CLASSIFICATION OF POSSIBLE TOPOLOGIES OF THE FTC

	Shunt	Series	Cascaded		
			Fractional rated	Direct AC–AC	Indirect AC–AC
Connection Scheme of IC and the connected system(s)	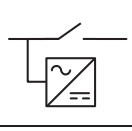	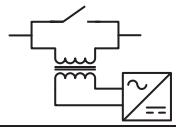	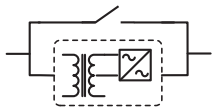		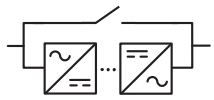
Example(s)	Intelligent Connection Agent [25]	Unified Power Quality Conditioner [30], Distributed Power-flow Controller [31]	Controllable Network Transformer [32], Power Router [33], Hybrid Transformer [34]	Matrix converters [35], converters with AC-link [36], [37], Variable Frequency Transformer [38]	Converters with DC-link [22], [29], [40]–[42], Smart Transformers [20], Solid-state Transformer [39]
Pre-synchronization	√	√	√	√	√
Asynchronous connection	×	√	√	√	√
Direct Power Flow Control	×	Limited	Limited	√	√
Grid Decoupling	×	×	×	×	√
Auxiliary Services	Fair	Fair	Limited	Limited	Good

in Table III. Note that the series–shunt type is considered as a special case of series type here.

Among the typical ICs, the shunt type [25] is a special one that contributes to the presynchronization but cannot directly control the power dispatch through the interface; some energy storage (ES) is required to complete the presynchronization [42]. The series type [30], [31] and fractional-rated converters integrated with transformers [32]–[34] can start to work in the ACM, but a larger rated capacity is required to interconnect two networks with different frequencies. Matrix converters and their derivative topologies with ac-links [35]–[37] can be employed to generate asynchronous interfaces. They may save space and weight by eliminating the dc-link, but this comes at the cost of higher power couplings between two sides and a poorer voltage transfer ratio; also, their efficiency for low-frequency applications is relatively low [35]. The variable frequency transformer [38] is bulky, costly, and has a slow dynamic response, making it unsuitable for the distribution networks. In indirect ac–ac converters, the presence of dc-link is critical for isolating disturbances, decoupling power flow, and reducing control complexity. As for multistage converters, such as solid-state or smart transformers [20], [39], although a medium-frequency transformer could be built with a somewhat higher efficiency than a low-frequency one, the losses of the additional conversion stages result in a lower overall efficiency [39], so they are superior only in connecting several ac and dc networks with different voltage levels. The back-to-back (B-to-B) voltage-source converter with two conversion stages [22], [29], [40]–[42], on the other hand, can achieve a better balance between the controllability, power losses, and cost, and is, hence, recommended as a choice for the general-purpose FTC. It should be noted that simplified dc-link converter topologies [40], [41] reduce the number of switching devices at the price of higher voltage stresses on them, which may not result in a reduced total cost.

The abovementioned comparison of possible topologies is simply a theoretical analysis for the FTC to be built; any existing asset near the grid interface could be modified to perform certain functions of the FTC.

III. CONTROL OF GENERAL-PURPOSE FTC

A. Basic Ideas

The primary functions of the FTC are PFC in the ACM and presynchronization control (PSC) during the transition to the SCM. These are also the reasons why the FTC could free microgrid from communication links, allowing autonomous control

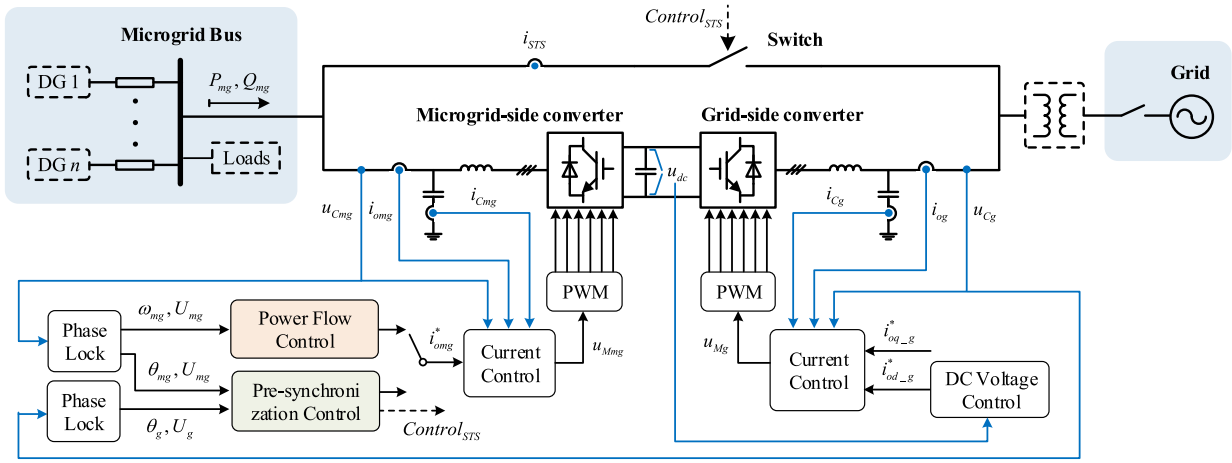

Fig. 3. Control block diagram of a general-purpose FTC connecting a microgrid and the utility grid.

and power dispatch. The control methods must be derived from the steady-state characteristics of the connected microgrid(s).

Normally, some small-scale RESs in the target microgrid are controlled as grid-feeding sources, and their dynamics can be neglected here since they behave like negative loads and can hardly affect the bus voltage, while the majority of DGs are controlled under different forms of droop control in order to ensure their ability to cooperatively support the bus voltage in islanded modes, and there is at least a droop relation to calculate the frequency and voltage amplitude references for inner voltage control loop as

$$\omega^* = \omega_0 - k_p \cdot \left(\frac{\omega_f}{s+\omega_f} \cdot P - P_0 \right) \tag{1a}$$

$$E^* = E_0 - k_q \cdot \left(\frac{\omega_f}{s+\omega_f} \cdot Q - Q_0 \right) \tag{1b}$$

where ω_0 and E_0 are their nominal values, k_p and k_q are droop coefficients (inversely proportional to the capacity), ω_f is the cutoff frequency of the low-pass filters (LPFs), and P_0 and Q_0 are the nominal powers. The following could be noticed from (1).

1) The differences between DG output powers and nominal powers can be partially reflected in the frequency and voltage amplitude on the bus. The FTC could then optimize the power dispatch based on local measurements if P_0 and Q_0 reflect the desired output of each DG.
2) By controlling the power flow at the interface, the FTC may indirectly control the total output of DGs, and then, the microgrid frequency and voltage amplitude will be adjusted to realize presynchronization.

B. Control Architecture

The overall control block diagram of a B-to-B-type general-purpose FTC connecting a microgrid and the utility grid is shown in Fig. 3. The FTC under study consists of a B-to-B voltage-source converter, static switch, and optional low-frequency transformer for isolation. The B-to-B converter is controlled as a current source, so both sides use an inner control loop to track the current references and provide active damping, e.g., the proportional–integral (PI) controllers in d–q frame and active damping based on capacitor current feedback [43] are selected in this article. Without loss of generality, the microgrid-side converter takes the lead, generating the current references based on FTC control modes, whereas the grid-side converter follows it by regulating the dc voltage. Two basic PFC modes and one PSC mode are provided here.

1) PFC-1: The PFC-1 mode is enabled when the grid requires specific power support and the microgrid has sufficient capacity to provide it. In this case, the recommended power dispatch from upper level is available, and the reference immediately follows grid demands i_{d}^* to absorb power from the microgrid.

2) PFC-2: In the studied microgrid, the bus frequency, as previously stated, indicates the active power shortage (or surplus), while the voltage amplitude reflects the reactive power, allowing specially designed DGs to reach desired outputs when they are restored. Therefore, under the conditions that the utility grid is equivalent to a strong voltage source and capable of handling any load variation, the references will autonomously be determined by the frequency and amplitude of microgrid voltage as

$$i_{od\_\mathrm{mg}}^* = G_C^{om}(s)(\omega_{\mathrm{mg}}^* - \omega_{\mathrm{mg}}) \tag{2a}$$

$$i_{oq\_\mathrm{mg}}^* = G_C^{u}(s)(U_{\mathrm{mg}}^* - U_{\mathrm{mg}}) \tag{2b}$$

where $G_C^{om}(s)$ and $G_C^{u}(s)$ are the PI controllers to restore the microgrid frequency ω_{mg} and voltage amplitude U_{mg} measured from the phase-locked loop (PLL), and ω_{mg}^* and U_{mg}^* are their target values, which will be illustrated in Section V. The FTC that connects two microgrids can be controlled using similar rules [16]–[22], hence it will not be detailed here.

In normal situations, the active power is prioritized, and the remaining FTC capacity can be used for reactive power and harmonic compensation. However, a heavy reactive load can sometimes limit the active power output of DG, and hence limit the utilization of RES. In this case, the DG will decrease its output voltage amplitude to reduce the reactive power it shares; the FTC can then detect an irregular voltage deviation and

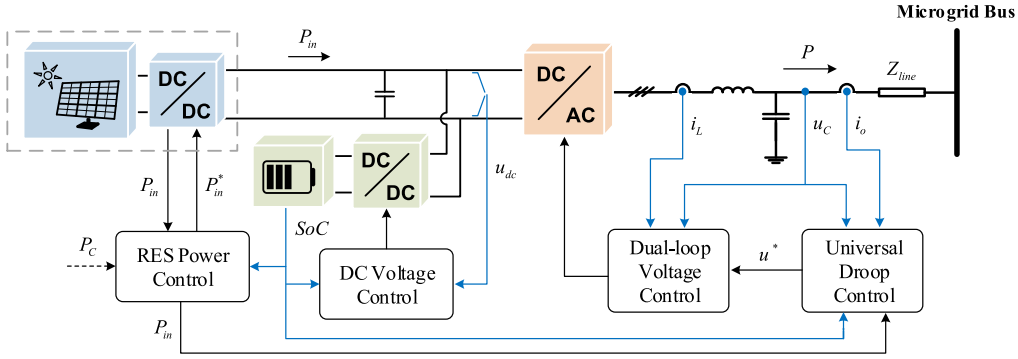

Fig. 4. Control of the RES, ES, and VSI in each DG.

switch to reactive power compensation as a priority to restore the voltage to a reasonable range [21].

3) PSC: The microgrid voltage should be synchronized with the grid before the FTC transfers to the SCM to reduce its operating losses; therefore, the phase and voltage amplitude differences are fed into PI controllers to establish a power dispatch as

$$i^*_{od\_\mathrm{mg}} = G^{\mathrm{th}}_C(s)(\theta_g - \theta_{\mathrm{mg}}) \tag{3a}$$

$$i^*_{oq\_\mathrm{mg}} = G^{u}_C(s)(U_g - U_{\mathrm{mg}}) \tag{3b}$$

where $G^{\mathrm{th}}_C(s)$ is the PI controller for phase synchronization, and ω_g and U_g are the grid frequency and voltage amplitude. Then after some time, the FTC controller will send a close demand to the switch when the synchronization conditions for phase, frequency, and amplitude differences are met, and the B-to-B converter can be shutdown gradually or continue to provide auxiliary services utilizing its capacity.

Because the main responsibility of the grid-side converter is to stabilize the dc voltage u_{dc} and maintain power balance, the current reference is set as

$$i^*_{od\_g} = -i^*_{od\_\mathrm{mg}} + G^{\mathrm{dc}}_C(s)(u_{\mathrm{dc}} - u^*_{\mathrm{dc}}) \tag{4}$$

where $G^{\mathrm{dc}}_C(s)$ is the PI controller for dc voltage regulation and u^*_{dc} is its nominal value. Because the reactive power on both sides of the B-to-B converter is decoupled, the reactive current reference can be set within its capability to meet grid demands.

Note that advanced control methods for current tracking and phase locking can certainly have better performance, and the frequency difference can also be included in (3a) to introduce another control degree of freedom for further improvement of dynamics [28]; however, only the simplest forms are mentioned here for understanding.

IV. Universal Control of DGs

In the target microgrid, each DG comprises an RES, certain ES, and a voltage-source inverter (VSI) that serves as the microgrid interface, as shown in Fig. 4. The RES converter is controlled to inject power into dc link, it can be a solar panel with dc–dc converter, a wind turbine with ac–dc converter, etc., while the ES bidirectional dc–dc converter is controlled to regulate the dc-link voltage with a reaction dead zone. Hence, the VSI can be controlled to regulate the terminal voltage so that the available power can be extracted.

The droop control in (1a) can achieve bus voltage regulation and power sharing among DGs in an islanded microgrid; however, in grid-connected mode, the output power of these DGs will be solely dictated by the bus frequency, making it impossible to fully exploit local RES generation. Fortunately, if the P_0 was changed to represent the DG's desired output active power, this issue could probably be solved in the SCM or the PFC-2. The state of charge (SoC) of ES, the power generated by RES, or even generation cost [44] and real-time pricing [45] need to be involved into the decision on P_0.

To be more precise, a universal droop control for the DGs considering RES generation and the SoC of ES is derived as

$$\omega^* = \omega_0 + k_{\mathrm{SoC}}(\mathrm{SoC} - \mathrm{SoC}_0) - k_p \cdot \frac{\omega_f}{s+\omega_f}(P - P_{\mathrm{in}}) \tag{5}$$

where k_{SoC} is the SoC droop coefficient, SoC_0 is the nominal value of SoC ($0 \le \mathrm{SoC} \le 1$), and P_{in} is the power generated by RES. As a result, four benefits can be obtained by introducing an SoC-related term.

1) Each DG can track its RES power if the bus frequency is regulated, making it applicable in both SCM and ACM (only the average SoCs differ a little).
2) By monitoring bus frequency and its changing rate, it is possible for the FTC to detect the average SoC and whether supply exceeds demand or demand exceeds supply.
3) The FTC capacity is no longer a constraint on frequency synchronization (compared with droop control).
4) The SoC of DGs can be balanced in any mode.

Rearrange (5), we have

$$\omega^* = \omega_0 - k_p \left(\frac{\omega_f}{s+\omega_f} \cdot P - \underbrace{\left(P_{\mathrm{in}} - \frac{k_{\mathrm{SoC}}}{k_p} \cdot (\mathrm{SoC} - \mathrm{SoC}_0) \right)}_{P_0} \right). \tag{6}$$

It can be noticed that (6) provides a possible expression for P_0 when compared with (1a). The VSI could then show certain characteristics of a grid-feeding converter over a longer time scale through changing P_0, yet behaving like a grid-supporting converter in a middle-frequency range to stabilize the system. Further, several existing research works took the SoC into

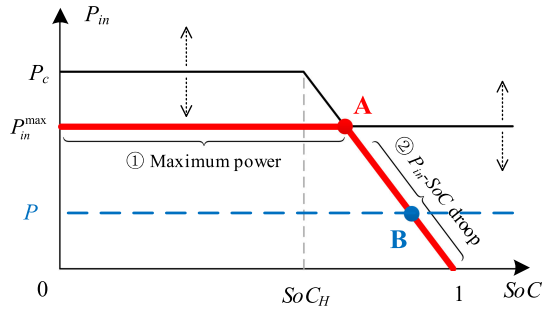

Fig. 5 Control curves of the RES.

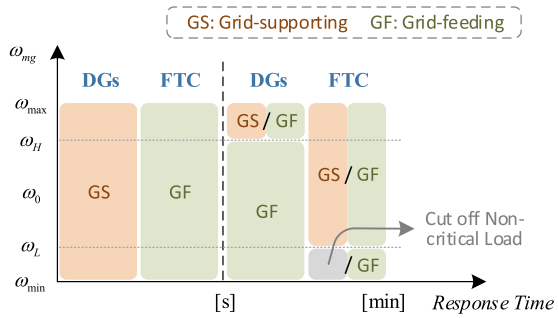

Fig. 6 Equivalent control modes of FTC and DGs on different time scales.

account [4], [46], [47], however, they were intended for SoC balancing in islanded microgrid instead of deriving a universal control for both modes; using SoC information to adjust droop slope will introduce additional nonlinear couplings into the system, and the performance of SoC balancing would be degraded by the frequency restoration of PSC-2. Furthermore, the power-related term in (5) is also essential, since it plays an important role in synchronization of DGs and coordination with the PSC, as well as helping to reduce the ES charging and discharging losses by forwarding the generation information.

As long as appropriate power is dispatched at the interface, the RES is normally managed at its highest output point to make the most of its potential. However, when islanding occurs, or the FTC adopts PFC-1, the SoCs of each DG may continue to rise until they hit an upper limit. Therefore, the RES generation must be limited in this case; also, it should be limited according to the DGs' capacities to ensure the power sharing, similar to a conventional droop control. To address these concerns, the reference power for RES is designed as

$$P_{\text{in}}^{*} = \min\left\{P_{\text{in}}^{\max},\quad P_C,\quad P_C \cdot \frac{1-\text{SoC}}{1-\text{SoC}_H}\right\} \tag{7}$$

where $P_{\text{in}}^{\max}$ is the maximum possible RES generation at this moment, e.g., the power calculated by maximum power point tracking algorithm for photovoltaics, P_C is the active power output capacity of DG, which is limited by its total capacity, output reactive, harmonic, and unbalance power, and SoC_H is the warning upper limit.

For a better understanding, the control curves of RES are depicted in Fig. 5. Due to the uncertain RES generation and various loads in the microgrid, both the P_C- and $P_{\text{in}}^{\max}$-curves are floating. If the supply exceeds demand, the SoC will continue to rise until it reaches the intersecting point A, at which point the P_{in} will begin to droop with the SoC and eventually rest at point B. In this situation, since the SoCs of DGs are equal in steady state, the active power will be shared proportionally to the P_C according to (7), which provides the microgrid with the most redundancy and the fairest manner for numerous prosumers.

Moreover, another possibility when islanding occurs is that local RES generations are insufficient to feed the microgrid loads and the SoCs are continuously lowering below a certain threshold SoC_L, at which point the FTC can capture this state through the bus frequency and then urgently absorb energy from the utility grid, or some noncritical loads has to be cutoff to ensure stable operation.

V. Coordination of FTC and DGs

In Sections III and IV, some basic control mechanisms of the FTC and DGs were described, while in this section, the coordination of them and its salient features are presented to construct a complete framework of an autonomous microgrid.

One of the core ideas of the proposed solution is to have the FTC and DGs coordinate in different ways on different time scales. As shown in Fig. 6, on a relatively short time scale, the DGs always behave like grid-supporting sources to cooperatively stabilize the microgrid voltage, whereas the FTC follows and works as a power source that merely affects the power balance. This design introduces several benefits, including increased reliability and redundancy, as well as improved immunity to islanding and other load disturbances. On a long time scale, however, the DGs exhibit certain characteristics of grid-feeding sources due to the SoC term, making their output power slowly track the average RES generation when the bus frequency is regulated below ω_H by the FTC or the grid; otherwise, the DGs will move toward the point B in Fig. 5 and degenerate into fully grid-supporting sources, as the SoC in (5) remains unchanged. To coordinate with the DGs, the FTC will gradually regulate the bus voltage to determine a reasonable power dispatch in the ACM; however, once upper level demands arrive, it will have to switch to grid-feeding mode, and the bus frequency may shift to another steady state after some time. The detailed control logic of the FTC under grid-connected mode is illustrated in Fig. 7.

As shown in Fig. 7, the FTC always starts from the ACM. The specific control mode is determined by whether there is a grid demand, a microgrid energy shortage or a permission for the SCM. Normally, the PFC-2 regulates the bus frequency to its nominal value, and the DGs' output powers and SoCs will likewise reach their desired values, while, when an energy shortage occurs in the case of grid demands, it stays at ω_L to feed the grid as far as possible. It should be noted that, to reduce transmission losses, a dead zone could be designed for the PFC-2 [17], [22]. Further, if the FTC capacity is insufficient to accomplish the control targets of PFC-1 or PFC-2, it could be detected by the FTC from its output power and the bus frequency. The PSC will then be activated to transfer the FTC to the SCM

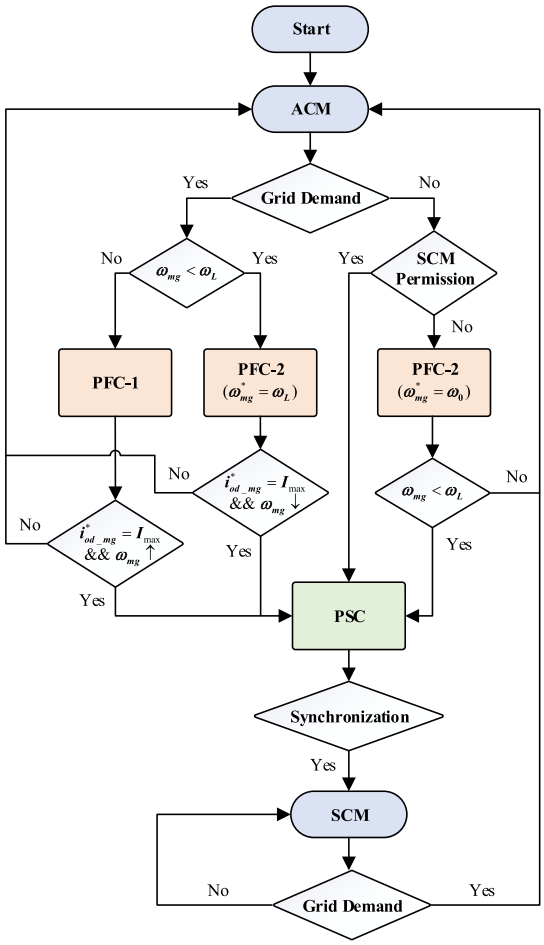

Fig. 7 Flowchart of the FTC under grid-connected mode.

after some time for confirmation, until the next grid demand arrives. If the energy shortage occurs in islanded mode, some noncritical loads has to be cutoff to ensure stable operation, as shown in Fig. 6.

It is worth noting that the active power flow is normally prioritized for DGs and FTC, unless the remaining FTC capacity is insufficient to handle an irregular voltage drop, as mentioned in Section III. In this case, the FTC must prioritize reactive power compensation and restore the voltage to a tolerable range, e.g., $0.93U^*_{\rm mg}$. This action can possibly cause a shortage, requiring the FTC to switch to the SCM.

As a result, an overall solution for autonomous microgrids is provided, which can achieve cooperative voltage supporting and accurate power sharing under islanded mode, reasonable power dispatch under grid-connected mode, and flexible and seamless mode transferring between them. Table IV compares the proposed method with some typical control methods in the literature. It can be noticed that the existing methods were focused on one or two particular aspects of the problem; thus, some only performed well in grid-connected or islanded mode, some failed to fully exploit the ability of the special converter, some might not coordinate it well with the DGs, and some were limited by the system topology or communication links, whereas the solution proposed in this article provides all the necessary characteristics of an autonomous microgrid.

VI. Modeling and Analysis

A. Small-Signal Modeling

A comprehensive small-signal model of the ac microgrids interconnected by B-to-B converter was presented in [48], which includes all details of the network dynamics, and the inner loops of DGs and FTC can be designed accordingly. However, as this article concentrates on the control methods of power dispatch and presynchronization in a generalized system, simplified models would be more appropriate. Given that the bandwidths of inner loops are much greater than those of power control loops, their tracking speed can be regarded high enough to ignore the dynamics.

To begin, an equivalent model of the studied microgrid is essential for investigating how power flow dynamics at the interface influence the connected microgrid. In this case, only the grid-forming DGs in this network controlled by (5) are involved since the grid-feeding sources behave like negative loads and are hardly influenced by the power flow.

Assuming that the system comprises n paralleled-connected DGs with similar dynamics, as shown in Fig. 3, the microgrid can be approximated by an equivalent droop source, and its droop coefficients and output impedance are given as

$$k_{p\rm mg} \approx 1/\sum_{i=1}^{n}\frac{1}{k_{pi}}, k_{q\rm mg} \approx 1/\sum_{i=1}^{n}\frac{1}{k_{qi}}, X_{\rm mg} \approx 1/\sum_{i=1}^{n}\frac{1}{X_i} \tag{8}$$

where X represents the reactance (assumed dominant) of the transmission line between DG output terminal and microgrid bus, and the subscript i denotes the ith DG. In most cases, the $X_{\rm mg}$ for distributed systems only needs to be roughly estimated, or it can be calculated by the Kron reduction method [49].

Also, the dynamics of ω are influenced by the SoC term in (5). Ignoring the power losses, the relation between P and SoC can be approximately derived as

$$\mathrm{SoC}(t) \approx \mathrm{SoC}(t_0) + \int_{t_0}^{t}\frac{1}{U_{\rm dc}C_e}(P_{\rm in} - P)dt \tag{9}$$

where C_e denotes the ES capacity and $U_{\rm dc}$ here represents the dc-link voltage of DG. Then, the small-signal form of (5) can be written as

$$\Delta\omega \approx -\left(k_p + \frac{k_{\rm SoC}}{U_{\rm dc}C_e}\frac{1}{s}\right)\cdot\frac{\omega_f}{s+\omega_f}\Delta P \tag{10}$$

where Δ denotes the small deviation of the respective variable. Therefore, an equivalent integral coefficient of the microgrid can be expressed as

$$K_{\rm SoCmg} \approx 1/\sum_{i=1}^{n}\frac{U_{{\rm dc}i}C_{ei}}{k_{{\rm SoC}i}}, \tag{11}$$

which indicates the dynamics brought on by the SoC term.

Since a standard PLL is used to detect the frequency and phase information here, its dynamics can be represented by a

TABLE IV
COMPARISON OF TYPICAL CONTROL STRATEGIES

Characteristics of Autonomous Microgrid		[10]	[16]–[19] and [21]	[20]	[22]	[23] and [24]	[25] and [26]	[5] and [27]	[28] and [29]	Proposed Method
Islanded Mode	DG Cooperative Voltage Supporting	√	√	×	Limited	×	×	√	√	√
	Reasonable DG Power Sharing	√	√	√	Limited	×	×	√	×	√
Asynchronous Connection Mode	Power Dispatch	×	√	√	√	√	×	×	×	√
	Autonomous Power Dispatch	×	√	√	√	×	×	×	×	√
Synchronous Connection Mode	Full Utilization of Local RES Generation	×	×	√	×	√	√	√	√	√
Flexible Mode Transfer	Seamless Presynchronization	√	×	×	×	√	√	√	√	√
	Immunity to Islanding	√	√	×	√	×	Limited	√	√	√
Independence of Communication		√	√	√	√	√	√	×	Limited	√

second-order transfer function as

$$G_{ED}^{\text{th}}(s) = \frac{U_0 k_p^{\text{pll}} s + U_0 k_i^{\text{pll}}}{s^2 + U_0 k_p^{\text{pll}} s + U_0 k_i^{\text{pll}}} \tag{12}$$

where k_p^{pll} and k_i^{pll} are the PI coefficients of the PLL, and U_0 is the bus voltage amplitude. If other error detection methods are adopted, (12) can be rewritten accordingly. Also, any filter for eliminating the effects of harmonics and ripples should also be considered here.

Finally, the small-signal models of studied system in PSC and PFC-2 are obtained in Fig. 8 by merging the dynamics of controllers, power stages, and error detection modules in (1)–(3), (5), (8), (11), and (12), where $\delta\theta$ and δU are the differences between the microgrid voltage and grid voltage, X_g is the grid impedance, and $G_{\text{LPF}}(s)$ represents the LPF in (1). Note that, due to the decoupling of reactive powers on two sides, the dotted line in Fig. 8(b) should only considered when the FTC absorbs reactive power from the grid for presynchronization. The reactive power control loop of PFC-2 is similar to that in Fig. 8(b), hence it is not depicted.

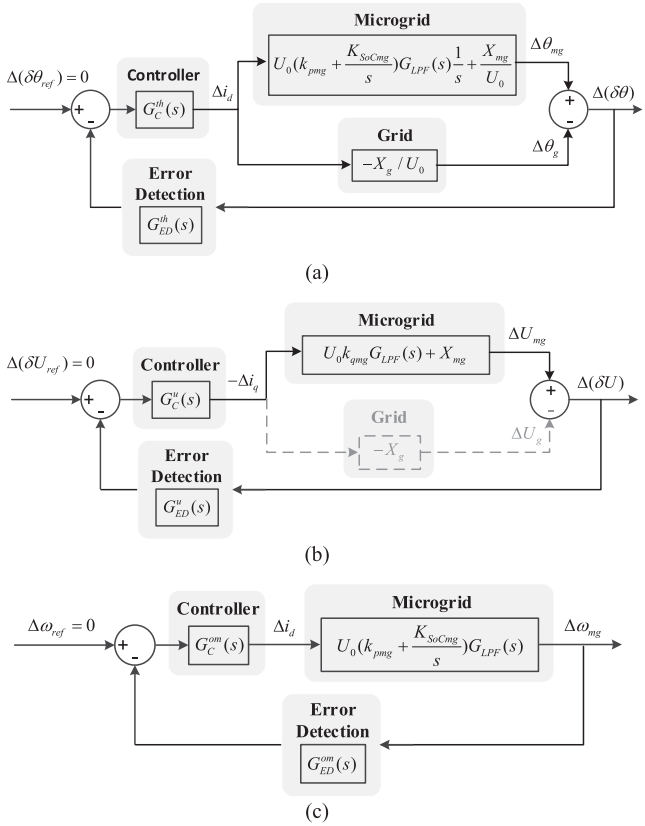

Fig. 8 Small-signal model of (a) phase synchronization loop of PSC, (b) amplitude synchronization loop of PSC, and (c) active power control loop of PFC-2.

B. Case Analysis and Parameter Design

Considering the PI controllers under PSC and PFC-2 have significant impacts on system stability and dynamic response, the root loci of each control mode when PI parameters change are plotted, and the zoomed-in figures of dominant poles are shown in Figs. 9–11, respectively. The parameters are chosen consistent with the simulations in Table V.

First, in Fig. 9, the real parts of dominant pole or poles are around -1, and in Fig. 10, they are around -10, which indicate that the phase and amplitude synchronization loops of PSC have different response speeds, and the phase difference is usually what determines the total time required. Furthermore, because dominant poles respond to changes in PI parameters in different ways, a careful compromise must be reached. They should be placed as far away from the imaginary axis as possible to optimize system stability and dynamic response; they are best positioned on the real axis to avoid unnecessary overshoots caused by an underdamped mode. Therefore, the intersection point, e.g., A or B, is a reasonable choice, because if the parameter is increased further, at least one pole will shift toward the imaginary axis. Then, we can fix this parameter and change the other one, and repeat this until they are the best match for each other. Finally, a proper design of the controller can be obtained through the root loci.

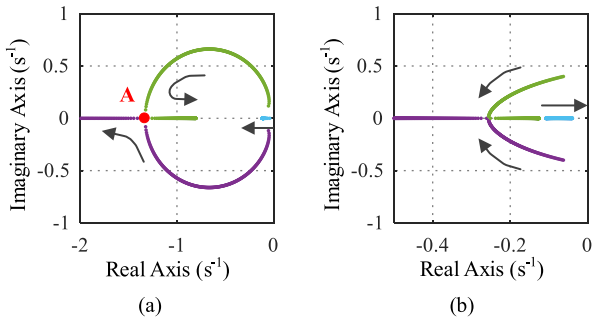

Fig. 9. Root loci of phase synchronization loop of PSC. (a) $k_p^{\text{th}} = 200$, $k_i^{\text{th}} = 1$–5000. (b) $k_i^{\text{th}} = 200$, $k_p^{\text{th}} = 1$–5000.

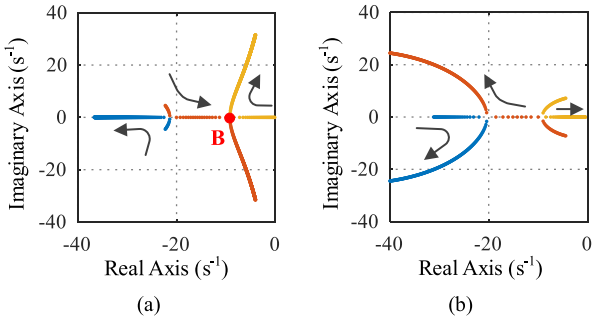

Fig. 10. Root loci of amplitude synchronization loop of PSC. (a) $k_p^u = 3$, $k_i^u = 1$–500. (b) $k_i^u = 30$, $k_p^u = 1$–50.

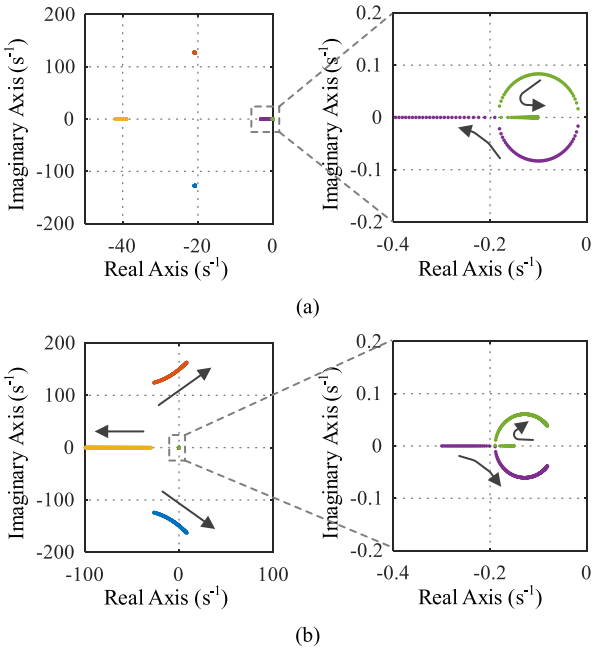

Fig. 11. Root loci of active power control loop of PFC-2. (a) $k_p^{\text{om}} = 500$, $k_i^{\text{om}} = 1$–5000. (b) $k_i^{\text{om}} = 500$, $k_p^{\text{om}} = 1$–5000.

Moreover, a pair of poles around $(-0.2, 0)$ can be seen in Fig. 11, indicating that the PFC-2 has a very slow mode due to the influence of SoC. However, they are not always dominant; as shown in Fig. 11(b), there is another pair of poles sensitive to the variations of k_p^{om}, and they may cross the imaginary axis and move to the right-half plane as k_p^{om} increases; therefore, k_p^{om} has to strictly constrained for stability considerations.

TABLE V
MAIN PARAMETERS OF SIMULATIONS AND EXPERIMENTS

Description	Simulation	Experiment
DC link voltage	$V_{dc} = 1000$ V	$V_{dc} = 400$ V
Nominal line voltage	$E_0 = 537$ V	$E_0 = 200$ V
Nominal frequency	$\omega_0 = 50*2\pi$ rad/s	
Switching frequency	$f_s = 12.5$ kHz	
L–C filter	$L_f = 2.7$ mH, $R_f = 0.01\ \Omega$, $C_f = 30\ \mu$F	
Grid voltage	$U_g = 520$ V	$U_g = 198$ V
Grid frequency	$\omega_g = 50*2\pi$ rad/s	
Cutoff frequency of LPFs	$\omega_f = 30$ rad/s	$\omega_f = 60$ rad/s
Active power droop	$k_p =$ 1e-5	$k_p =$ 5e-5
Reactive power droop	$k_q =$ 1e-3	$k_q =$ 1e-4
ES coefficient	$K_{SoC} =$ 1e-6	$K_{SoC} =$ 5e-7
Nominal SoC	$SoC_0 = 50\%$	
P-I coefficients of PLL	$k_p^{pll} = 0.1$, $k_i^{pll} = 30$	$k_p^{pll} = 0.03$, $k_i^{pll} = 0.2$
P-I coefficients of $G_C^{dc}(s)$	$k_p^{dc} = 4$, $k_i^{dc} = 40$	$k_p^{dc} = 1$, $k_i^{dc} = 3$
P-I coefficients of $G_C^{th}(s)$	$k_p^{th} = 200$, $k_i^{th} = 200$	$k_p^{th} = 5$, $k_i^{th} = 1.5$
P-I coefficients of $G_C^{u}(s)$	$k_p^{u} = 3$, $k_i^{u} = 50$	$k_p^{u} = 0.15$, $k_i^{u} = 0.3$
P-I coefficients of $G_C^{om}(s)$	$k_p^{om} = 500$, $k_i^{om} = 1000$	$k_p^{om} = 15$, $k_i^{om} = 150$

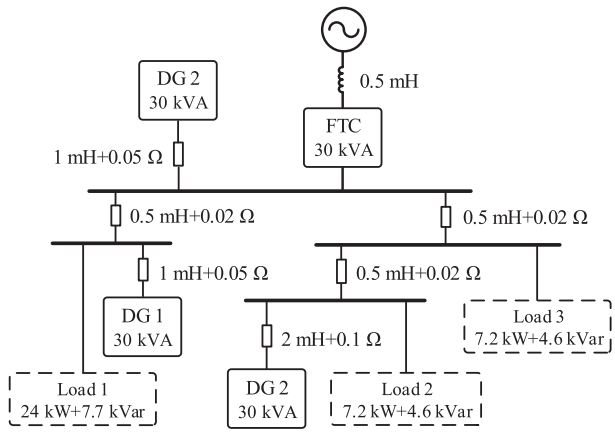

Fig. 12. Topology of the simulation circuit.

VII. VERIFICATIONS

A. Simulation Verifications

A typical general-purpose FTC connecting a distributed ac microgrid to the utility grid was simulated in PSCAD/EMTDC environment. The simulation topology and load information are provided in Fig. 12. The main simulation parameters are listed in Table V, with the first group being common to both the DG and FTC, and the second and third groups being unique to one of them.

Fig. 13 shows simulation results when the FTC works in the ACM and the PFC-2 starts at $t = 1$ s. The *SoC*s are assumed to be the nominal value to highlight the tracking accuracy. As

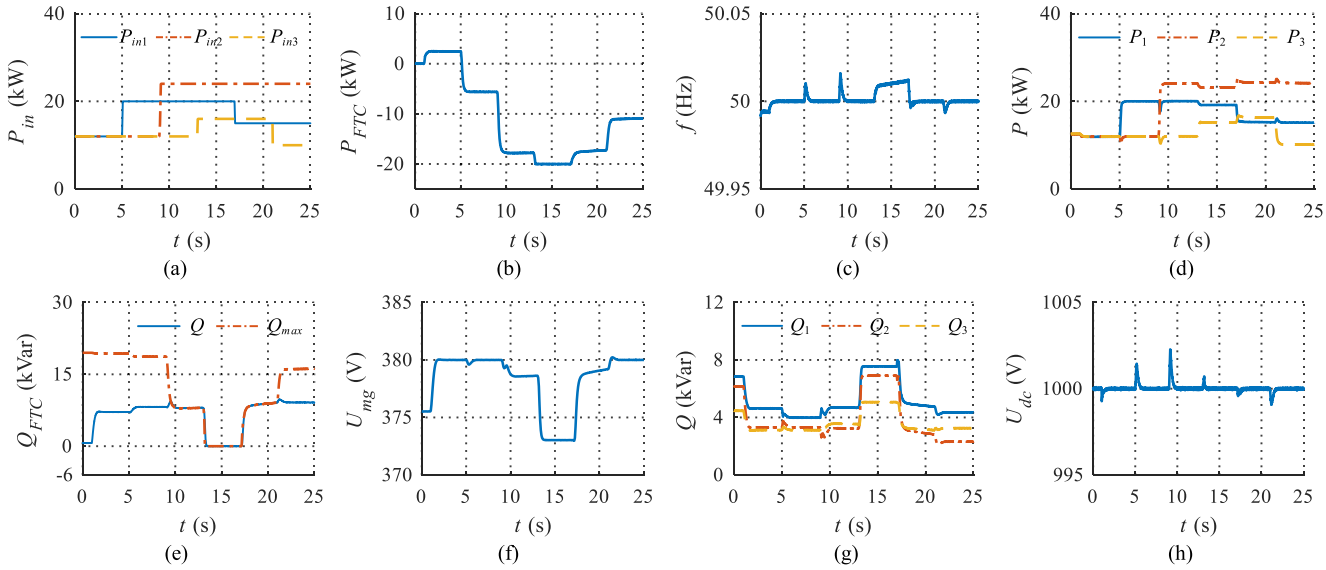

Fig. 13. Simulation waveforms of (a) RES power, (b) FTC active power, (c) microgrid frequency, (d) DG active power, (e) FTC reactive power, (f) bus voltage amplitude, (g) DG reactive power, and (h) dc-link voltage of FTC in the PFC-2.

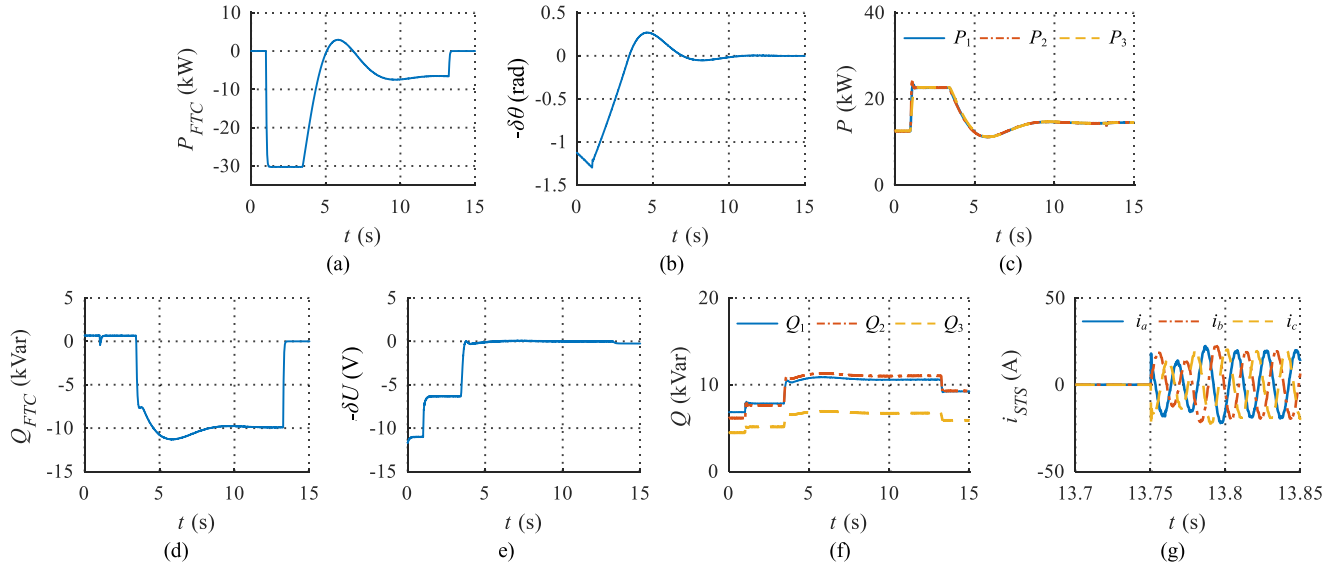

Fig. 14. Simulation waveforms of (a) FTC active power, (b) phase difference, (c) DG active power, (d) FTC reactive power, (e) voltage amplitude difference, (f) DG reactive power, and (g) bypass switch currents in the PSC.

shown in Fig. 13(b) and (c), the FTC autonomously controls the power dispatch by regulating the bus frequency; then, as shown in Fig. 13(a), the RESs change their generations one by one, and the FTC can respond to these changes by outputting varying power to make the most of local generations within its capacity, with an exception that at $t = 13$ s, the FTC reaches its preset maximum output active power. As a result, the DGs' output powers in Fig. 13(d) can track their RES generation in Fig. 13(a) as far as possible, although they are controlled as grid-supporting sources. Also, in Fig. 13(e)–(g), the residual capacity of FTC [indicated by the dotted line in Fig. 13(e)] is used to compensate reactive power and regulate bus voltage. It will only prioritize reactive power in case of irregular voltage drops. Because the dc-link voltage in Fig. 13(h) is regulated by the grid-side converter, all active power is transferred between the two sides and no ES is required. Note that the power tracking performance of PFC-1 could also be verified by Fig. 13(b) and (f), thus it was not presented.

Fig. 14 shows the results when the FTC needs to transfer to the SCM and the PSC starts at $t = 1$ s. As shown in Fig. 14(a) and (b), the FTC uses its entire capacity to deal with phase synchronization first by dispatching active power. Because it is substantially slower than the amplitude synchronization, as illustrated in Section VI, and outputting reactive power too early would reduce available active power capacity, slowing the process. After several seconds, its active power is reduced to maintain the phase difference at zero, and the residual capacity is used to synchronize the amplitudes by controlling reactive

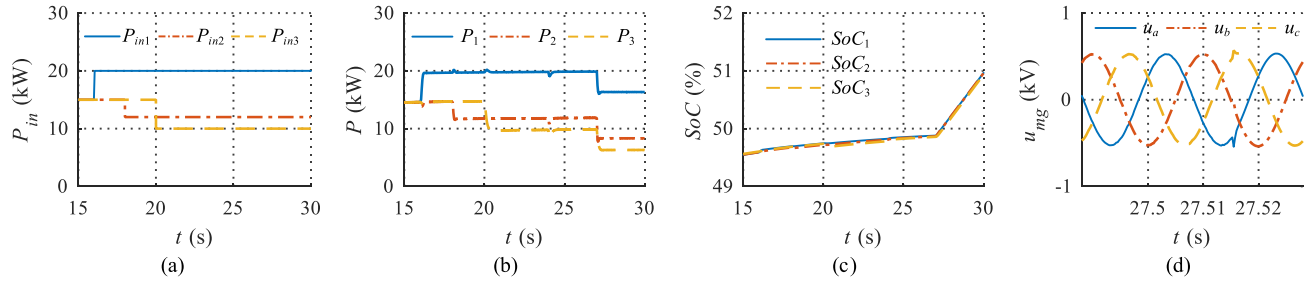

Fig. 15. Simulation waveforms of (a) RES power, (b) DG active power, (c) SoC, and (d) microgrid voltages in the SCM and in the case of islanding.

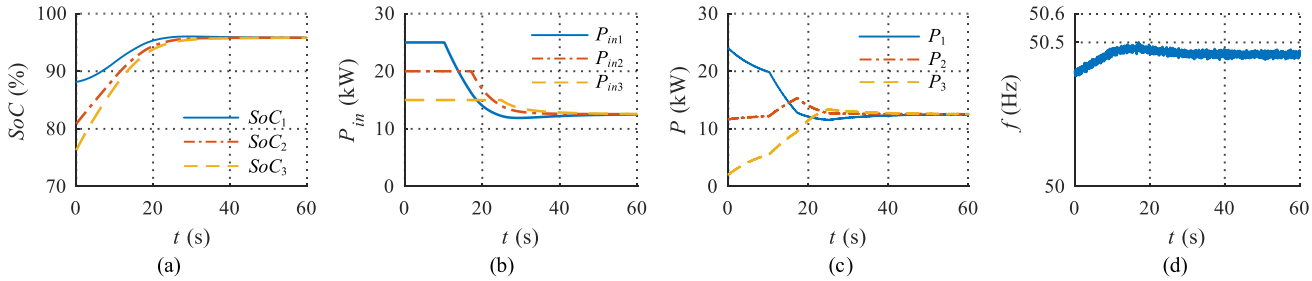

Fig. 16. Simulation waveforms of (a) SoC, (b) RES power, (c) DG active power, and (d) microgrid frequency in islanded mode.

power, as shown in Fig. 14(d) and (e). Finally, the synchronization conditions are met (phase, amplitude, and frequency differences are within acceptable ranges) at around $t = 13.75$ s, and the bypass switch is then closed, switching the FTC to the SCM. The waveforms of inrush currents on the switch is depicted in Fig. 14(g) to prove a smooth transition.

After switching to the SCM, the bus voltage frequency is clamped by the utility grid. As a result, the universal DG control gradually regulates the SoC of each DG to its nominal value, and then each DG's output will follow its generation, as shown in Fig. 15(a)–(c). At $t = 16$ s, the RESs change their generations one by one, and the DGs provide equally good tracking performance as in the PFC-2. At around $t = 27$ s, an unscheduled islanding occurs and the power flow between the microgrid and the grid is blocked, and, thanks to the grid-supporting characteristic provided by the universal DG control, the DGs naturally decrease their output power to supply the local demands cooperatively, just as if they were undergoing a normal load change, as illustrated by the waveforms of bus voltage in Fig. 15(d). Note that, although the proposed solution is immune to islanding, in the case of scheduled islanding, the FTC can switch to the ACM first, then gradually decrease the power dispatch to mimic a ramp load change; this action could certainly mitigate its impacts on the microgrid, while it may not be a necessary step before islanding.

The performance of the universal DG control in islanded mode is verified by Fig. 16. It is assumed that supply exceeds demand in this case, and the initial SoCs and RES generations of DGs are set to be different to highlight the convergence process. When islanding occurs, the ESs are continuously charged until the *SoC*s approach the upper limit in sequence, after which the DGs gradually decrease their generations to a proper value one by one, as shown in Fig. 16(a) and (b); as a result, their output powers also converge to the same value in Fig. 16(c). Finally, the system reaches a steady state in which the SoCs are balanced and local loads are shared according to their capacities rather than their generations, providing the microgrid with the most redundancy and the fairest manner for numerous prosumers.

B. Experiment Verifications

To further verify the effectiveness of FTC control modes, downscaled experiments were carried out in our lab on an FTC prototype that connected a simplified microgrid to a grid simulator, as shown in Fig. 17. The major components of the experiment platform were four three-phase inverters with *L*–*C* filters and line impedances, two of which were connected back to back and combined with switches and isolation transformer to form an FTC. The control algorithms were implemented using DSPs (TMS320F28335) on each inverter, and some of the waveforms below were exported by the digital-to-analog converters and then displayed on the oscilloscopes. Main parameters are also included in Table V.

The first case demonstrates how the PFC-2 autonomously manages power dispatch and restores the microgrid frequency, as well as how it reacts to RES generation variations. As shown in Fig. 18, when the PFC-2 starts, a frequency deviation of about 0.1 Hz is detected by the FTC and gradually regulated to zero by injecting power into the microgrid; after that, a step change in RES generation is about to increase the frequency, but the FTC change the output power to offset its influence in one second.

The experiment waveforms of microgrid and grid voltages, as well as FTC output powers, before and after the PSC, are

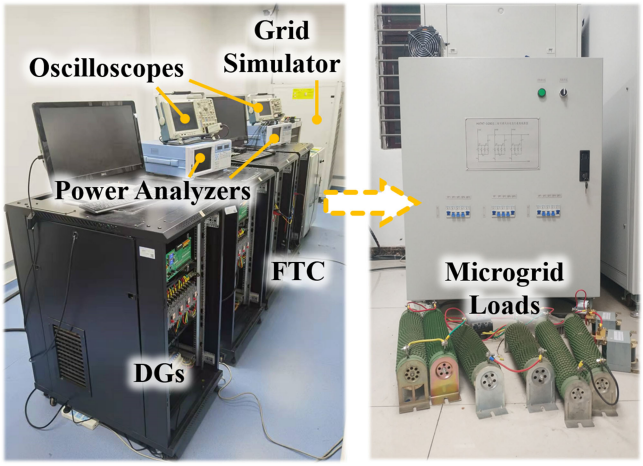

Fig. 17. Experiment platform: microgrid, grid, and FTC prototype.

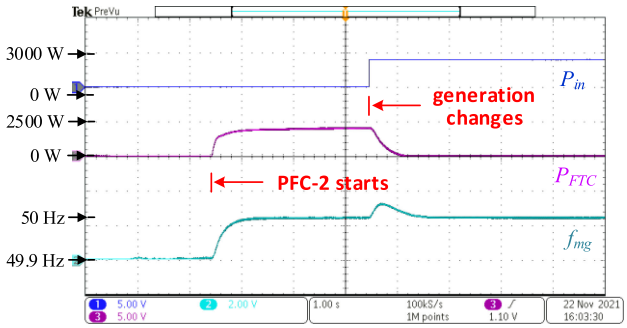

Fig. 18. Experimental waveforms of DG reference power, FTC output power, and microgrid frequency when PFC-2 starts and then a DG changes its generation (P_0 /P_{FTC}: 2500 W/div, f_{mg}: 0.08 Hz /div).

depicted in Fig. 19. By controlling the active and reactive power flow, the FTC eliminates an initial frequency mismatch of roughly 0.1 Hz and a phase difference of about 45° by managing active and reactive power flow, resulting in a seamless transition to the SCM. These two scenarios confirm the results of previous simulations.

Furthermore, the response time of mechanical switches is about 10–100 ms; static switches have a response time of less than 1 ms and can, thus, be neglected, however their leakage currents necessitate their use in conjunction with mechanical switches. Therefore, in some conditions, the actions of the IC and bypass switch need to be well coordinated to improve the smoothness of transient process. If the IC stops earlier, there will be larger inrush currents, while if switch is closed earlier, there will be some currents circulating inside the FTC, as shown by the inrush currents in Fig. 20(a). It also implies that, when both sides of the FTC are not stopped after the PSC and employed to provide auxiliary services in the SCM, further circulating current suppression techniques will be required. To compensate for these impacts introduced by switch action time, we can simply trigger the IC with a certain time delay, as the microgrid operates in a steady state synchronized with the grid after the PSC. In

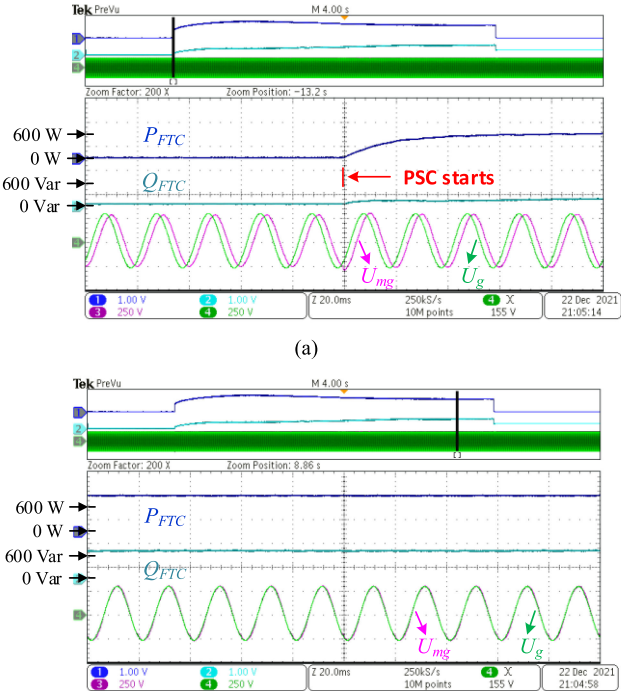

Fig. 19. Experimental waveforms of microgrid and grid voltages, and FTC output powers (a) before and (b) after PSC (P_{FTC}: 600 W/div, Q_{FTC}: 600 Var/div, u_{mg}/u_g: 250 V/div).

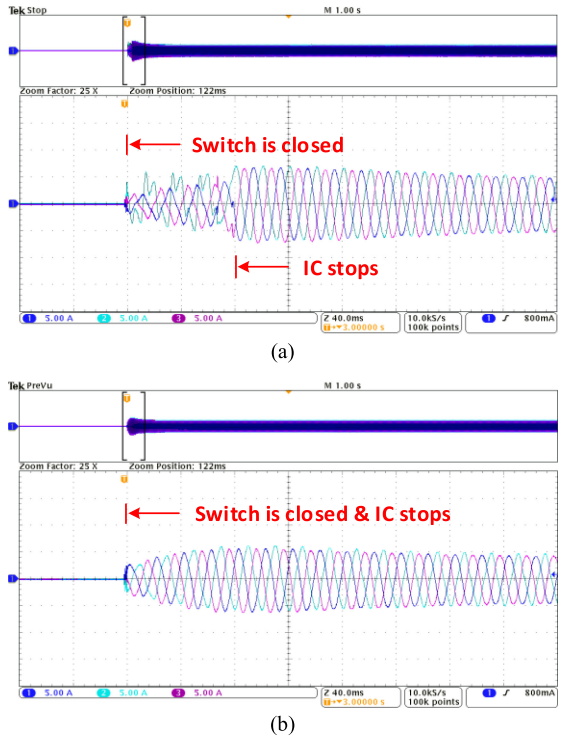

Fig. 20. Experimental waveforms of inrush currents on bypass switch when the switch and FTC act (a) with a time difference or (b) at the same time (i_{STS}: 5 A/div).

Fig. 20(b), the triggering timings are properly set, resulting in a smoother transition.

VIII. Conclusion and Future Work

Based on the scenario of autonomous microgrids, the FTC and its basic knowledge are introduced in this study. As an example, a general-purpose FTC and a universal DG control strategy are presented to provide appropriate power dispatch and flexible mode transition in a communication-free design. As a result, a fully autonomous microgrid involving multiple prosumers is obtained. Also, generalized small-signal models and comprehensive case studies are provided to analyze the target system and demonstrate the effectiveness.

Simple and cost-effective operation rules, as well as high interoperability with existing assets, makes the FTC promising for distributed microgrid applications. Based on the blueprint described in this article, future research will mainly focus on advanced controller design, simplified topologies, and control strategies for normally islanded and normally connected FTCs, and coordinated control of the FTCs.

References

[1] S. Kulkarni *et al.*, "Enabling a decentralized smart grid using autonomous edge control devices," *IEEE Internet Things J.*, vol. 6, no. 5, pp. 7406–7419, Oct. 2019.

[2] A. Bani-Ahmed, M. Rashidi, A. Nasiri, and H. Hosseini, "Reliability analysis of a decentralized microgrid control architecture," *IEEE Trans. Smart Grid*, vol. 10, no. 4, pp. 3910–3918, Jul. 2019.

[3] F. Nejabatkhah and Y. W. Li, "Overview of power management strategies of hybrid AC/DC microgrid," *IEEE Trans. Power Electron.*, vol. 30, no. 12, pp. 7072–7089, Dec. 2015.

[4] J. M. Guerrero, J. C. Vasquez, J. Matas, M. Castilla, and L. Garcia de Vicuna, "Control strategy for flexible microgrid based on parallel line-interactive UPS systems," *IEEE Trans. Ind. Electron.*, vol. 56, no. 3, pp. 726–736, Mar. 2009.

[5] J. Kim, J. M. Guerrero, P. Rodriguez, R. Teodorescu, and K. Nam, "Mode adaptive droop control with virtual output impedances for an inverter-based flexible AC microgrid," *IEEE Trans. Power Electron.*, vol. 26, no. 3, pp. 689–701, Mar. 2011.

[6] M. Gao, M. Chen, B. Zhao, B. Li, and Z. Qian, "Design of control system for smooth mode-transfer of grid-tied mode and islanding mode in microgrid," *IEEE Trans. Power Electron.*, vol. 35, no. 6, pp. 6419–6435, Jun. 2020.

[7] M. Karimi-Ghartemani, "Universal integrated synchronization and control for single-phase DC/AC converters," *IEEE Trans. Power Electron.*, vol. 30, no. 3, pp. 1544–1557, Mar. 2015.

[8] I. J. Balaguer, Q. Lei, S. Yang, U. Supatti, and F. Z. Peng, "Control for grid-connected and intentional islanding operations of distributed power generation," *IEEE Trans. Ind. Electron.*, vol. 58, no. 1, pp. 147–157, Jan. 2011.

[9] A. Kumar, A. Mohapatra, and S. N. Singh, "Sequence measurement-based islanding detection of DGs in microgrid with enhanced power quality," *IEEE Trans. Instrum. Meas.*, vol. 70, Aug. 2021, Art. no. 6504011.

[10] T. L. Vandoorn, B. Meersman, J. D. M. De Kooning, and L. Vandevelde, "Transition from islanded to grid-connected mode of microgrids with voltage-based droop control," *IEEE Trans. Power Syst.*, vol. 28, no. 3, pp. 2545–2553, Aug. 2013.

[11] X. Meng, Z. Liu, H. Zheng, and J. Liu, "A universal controller under different operating states for parallel inverters with seamless transfer capability," *IEEE Trans. Power Electron.*, vol. 35, no. 9, pp. 9794–9812, Sep. 2020.

[12] M. Kwon, S. Park, C. Oh, J. Lee, and S. Choi, "Unified control scheme of grid-connected inverters for autonomous and smooth transfer to stand-alone mode," *IEEE Trans. Power Electron.*, vol. 37, no. 1, pp. 416–425, Jan. 2022.

[13] Y. Li, D. M. Vilathgamuwa, and P. C. Loh, "Design, analysis, and real-time testing of a controller for multibus microgrid system," *IEEE Trans. Power Electron.*, vol. 19; no. 19, pp. 1195–1204, Sep. 2004.

[14] H. Xu *et al.*, "Synchronization strategy of microgrid from islanded to grid-connected mode seamless transfer," in *Proc . IEEE Int. Conf. IEEE Region 10*, 2013, pp. 1–4.

[15] E. Pashajavid, F. Shahnia, and A. Ghosh, "Development of a self-healing strategy to enhance the overloading resilience of islanded microgrids," *IEEE Trans. Smart Grid*, vol. 8, no. 2, pp. 868–880, Mar. 2017.

[16] A. Ordono, E. Unamuno, J. A. Barrena, and J. Paniagua, "Interlinking converters and their contribution to primary regulation: A review," *Int. J. Elect. Power Energy Syst.*, vol. 111, pp. 44–57, Oct. 2019.

[17] X. Hou, K. Sun, N. Zhang, F. Teng, X. Zhang, and T. Green, "Priority-driven self-optimizing power control scheme for interlinking Conver-ters of hybrid AC/DC microgrid clusters in decentralized manner," *IEEE Trans. Power Electron.*, vol. 37, no. 5, pp. 5970–5983, May 2022.

[18] P. Yang, M. Yu, Q. Wu, N. Hatziargyriou, Y. Xia, and W. Wei, "Decentralized bidirectional voltage supporting control for multi-mode hybrid AC/DC microgrid," *IEEE Trans. Smart Grid*, vol. 11, no. 3, pp. 2615–2626, May 2020.

[19] J. Wang, C. Jin, and P. Wang, "A uniform control strategy for the interlinking converter in hierarchical controlled hybrid AC/DC microgrids," *IEEE Trans. Ind. Electron.*, vol. 65, no. 8, pp. 6188–6197, Aug. 2018.

[20] G. De Carne, G. Buticchi, Z. Zou, and M. Liserre, "Reverse power flow control in a ST-Fed distribution grid," *IEEE Trans. Smart Grid*, vol. 9, no. 4, pp. 3811–3819, Jul. 2018.

[21] I. U. Nutkani, P. C. Loh, and F. Blaabjerg, "Distributed operation of interlinked AC microgrids with dynamic active and reactive power tuning," *IEEE Trans. Ind. Applicat.*, vol. 49, no. 5, pp. 2188–2196, Sep. 2013.

[22] N. Nasser and M. Fazeli, "Buffered-microgrid structure for future power networks; a seamless microgrid control," *IEEE Trans. Smart Grid*, vol. 12, no. 1, pp. 131–140, Jan. 2021.

[23] W. Cao, J. Wu, N. Jenkins, C. Wang, and T. Green, "Operating principle of soft open points for electrical distribution network operation," *Appl. Energy*, vol. 164, pp. 245–257, Feb. 2016.

[24] S. Giacomuzzi, G. De Carne, S. Pugliese, G. Buja, M. Liserre, and A. Kazerooni, "Synchronization of low voltage grids fed by smart and conventional transformers," *IEEE Trans. Smart Grid*, vol. 12, no. 4, pp. 2941–2951, Jul. 2021.

[25] J. Rocabert, G. M. S. Azevedo, A. Luna, J. M. Guerrero, J. I. Candela, and P. Rodríguez, "Intelligent connection agent for three-phase grid-connected microgrids," *IEEE Trans. Power Electron.*, vol. 26, no. 10, pp. 2993–3005, Oct. 2011.

[26] J. Chen, S. Hou, and J. Chen, "Seamless mode transfer control for master–slave microgrid," *IET Power Electron.*, vol. 12, pp. 3158–3165, 2019.

[27] I. Serban, "A control strategy for microgrids: Seamless transfer based on a leading inverter with supercapacitor energy storage system," *Appl. Energy*, vol. 221, pp. 490–507, Jul. 2018.

[28] S. Shah, H. Sun, D. Nikovski, and J. Zhang, "VSC-based active synchronizer for generators," *IEEE Trans. Energy Convers.*, vol. 33, no. 1, pp. 116–125, Mar. 2018.

[29] N. Bilakanti, D. Divan, and F. Lambert, "A novel approach for bumpless connection of microgrids with the grid," in *Proc. IEEE Decentralized Energy Access Solutions Workshop*, 2019, pp. 207–212.

[30] S. K. Khadem, M. Basu, and M. F. Conlon, "Intelligent islanding and seamless reconnection technique for microgrid with UPQC," *IEEE J. Emerg. Sel. Topics Power Electron.*, vol. 3, no. 2, pp. 483–492, Jun. 2015.

[31] Z. Yuan, S. W. H. de Haan, J. B. Ferreira, and D. Cvoric, "A FACTS device: Distributed power-flow controller (DPFC)," *IEEE Trans. Power Electron.*, vol. 25, no. 10, pp. 2564–2572, Oct. 2010.

[32] D. Das, D. M. Divan, and R. G. Harley, "Power flow control in networks using controllable network transformers," *IEEE Trans. Power Electron.*, vol. 25, no. 7, pp. 1753–1760, Jul. 2010.

[33] R. P. Kandula, A. Iyer, R. Moghe, J. E. Hernandez, and D. Divan, "Power router for meshed systems based on a fractionally rated back-to-back converter," *IEEE Trans. Power Electron.*, vol. 29, no. 10, pp. 5172–5180, Oct. 2014.

[34] S. Bala, D. Das, E. Aeloiza, A. Maitra, and S. Rajagopalan, "Hybrid distribution transformer: Concept development and field demonstration," in *Proc. IEEE Energy Convers. Congr. Expo.*, 2012, pp. 4061–4068.

[35] T. Friedli, J. W. Kolar, J. Rodriguez, and P. W. Wheeler, "Comparative evaluation of three-phase AC–AC matrix converter and voltage DC-link back-to-back converter systems," *IEEE Trans. Ind. Electron.*, vol. 59, no. 12, pp. 4487–4510, Dec. 2012.

[36] K. Mozaffari and M. Amirabadi, "A versatile family of partial-resonance inductive-ac-link universal converters," *IEEE Trans. Power Electron.*, vol. 34, no. 8, pp. 7292–7309, Aug. 2019.
[37] J. W. Kolar, T. Friedli, J. Rodriguez, and P. W. Wheeler, "Review of three-phase PWM AC–AC converter topologies," *IEEE Trans. Ind. Electron.*, vol. 58, no. 11, pp. 4988–5006, Nov. 2011.
[38] B. Bagen, D. Jacobson, G. Lane, and H. M. Turanli, "Evaluation of the performance of back-to-back HVDC converter and variable frequency transformer for power flow control in a weak interconnection," in *Proc. IEEE Power Eng. Soc. Gen. Meeting*, 2007, pp. 1–6.
[39] J. E. Huber and J. W. Kolar, "Solid-state transformers: On the origins and evolution of key concepts," *IEEE Ind. Electron. Mag.*, vol. 10, no. 3, pp. 19–28, Mar. 2016.
[40] C. Liu, B. Wu, N. R. Zargari, D. Xu, and J. Wang, "A novel three-phase three-leg AC/AC converter using nine IGBTs," *IEEE Trans. Power Electron.*, vol. 24, no. 5, pp. 1151–1160, May 2009.
[41] M. Heydari, A. Fatemi, and A. Yazdian Varjani, "A reduced switch count three-phase AC/AC converter with six power switches: Modeling, analysis, and control," *IEEE J. Emerg. Sel. Topics Power Electron.*, vol. 5, no. 4, pp. 1720–1738, Dec. 2017.
[42] S. M. Amrr Imdadullah, M. S. Jamil Asghar, I. Ashraf, and M. Meraj, "A comprehensive review of power flow controllers in interconnected power system networks," *IEEE Access*, vol. 8, pp. 18036–18063, 2020.
[43] J. He and Y. W. Li, "Generalized closed-loop control schemes with embedded virtual impedances for voltage source converters with LC or LCL filters," *IEEE Trans. Power Electron.*, vol. 27, no. 4, pp. 1850–1861, Apr. 2012.
[44] F. Chen *et al.*, "Cost-based droop schemes for economic dispatch in islanded microgrids," *IEEE Trans. Smart Grid,* vol. 8, no. 1, pp. 63–74, Jan. 2017.
[45] R. Jinsiwale and D. Divan, "Decentralized real-time pricing to achieve integrated transactive and physical grids," *IEEE Access,* vol. 7, pp. 132525–132541, 2019.
[46] Q. Wu, R. Guan, X. Sun, Y. Wang, and X. Li, "SoC balancing strategy for multiple energy storage units with different capacities in islanded microgrids based on droop control," *IEEE Trans. Emerg. Sel. Topics Power Electron.*, vol. 6, no. 4, pp. 1932–1941, Dec. 2018.
[47] X. Lu, K. Sun, J. M. Guerrero, J. C. Vasquez, and L. Huang, "State-of-Charge balance using adaptive droop control for distributed energy storage systems in DC microgrid applications," *IEEE Trans. Power Electron.*, vol. 61, no. 6, pp. 2804–2815, Jun. 2014.
[48] M. Naderi, Y. Khayat, Q. Shafiee, T. Dragicevic, H. Bevrani, and F. Blaabjerg, "Interconnected autonomous AC microgrids via back-to-back converters—Part I: Small-signal modeling," *IEEE Trans. Power Electron.*, vol. 35, no. 5, pp. 4728–4740, May 2020.
[49] F. Dorfler and F. Bullo, "Kron reduction of graphs with applications to electrical networks," *IEEE Trans. Circuits Syst. I. Reg. Papers*, vol. 60, no. 1, pp. 150–163, Jan. 2013.
[50] R. An, J. Liu, Z. Song, Z. Liu, and Y. P. Y. Deng, " A control method for flexible transfer converter to enable autonomous control of AC microgrids," in *Proc. IEEE Appl. Power Electron. Conf. Expo.*, 2022, pp. 1543–1550.

Ronghui An (Student Member, IEEE) received the B.S. degree in electrical engineering and automation in 2016 from Xi'an Jiaotong University, Xi'an, China, Where he is currently working toward the Ph.D. degree.

His research interests include coordinative control of distributed generations in microgrids, control and design of grid-interlinking converters, and emerging techniques for future power system.

Jinjun Liu (Fellow, IEEE) received the B.S. and Ph.D. degrees in electrical engineering from Xi'an Jiaotong University (XJTU), Xi'an, China, in 1992 and 1997, respectively.

He then joined the Electrical Engineering School, XJTU, as a Faculty. From late 1999 to early 2002, he was with the Center for Power Electronics Systems, Virginia Polytechnic Institute and State University, Blacksburg, VA, USA, as a Visiting Scholar. In late 2002, he was promoted to a Full Professor and then the Head of the Power Electronics and Renewable Energy Center, XJTU, which now comprises more than 20 faculty members and more than 200 graduate students and carries one of the leading power electronics programs in China. From 2005 to early 2010, he was an Associate Dean of Electrical Engineering School, XJTU, and from 2009 to early 2015, he was the Dean of Undergraduate Education, XJTU. He is currently a XJTU Distinguished Professor of power electronics. He coauthored three books (including one textbook), authored or coauthored more than 500 technical papers in peer-reviewed journals and conference proceedings, holds 70 invention patents (China/US/EU), and delivered for many times plenary keynote speeches and tutorials at IEEE conferences or China national conferences. His research interests include modeling, control, and design methods for power converters and electronified power systems, power quality control and utility applications of power electronics, and microgrids for sustainable energy and distributed generation.

Dr. Liu was the recipient of many governmental awards at national level or provincial/ministerial level for scientific research/teaching achievements, 2006 Delta Scholar Award, 2014 Chang Jiang Scholar Award, 2014 Outstanding Sci-Tech Worker of the Nation Award, 2016 State Council Special Subsidy Award, IEEE TRANSACTIONS ON POWER ELECTRONICS 2016 and 2021 Prize Paper Awards, and Nomination Award for the Grand Prize of 2020 Bao Steel Outstanding Teacher Award. He was the IEEE Power Electronics Society Region 10 Liaison and then China Liaison for ten years, he has been an Associate Editor for the IEEE TRANSACTIONS ON POWER ELECTRONICS since 2006, 2015–2019 Executive Vice President, and 2020-2021 Vice President of IEEE PELS. He was on the Board of China Electrotechnical Society 2012–2020 and was elected the Vice President in 2013 and the Secretary General in 2018 of the CES Power Electronics Society. He was the Vice President for International Affairs, China Power Supply Society (CPSS), from 2013 to 2021, and since 2016, the inaugural Editor-in-Chief of *CPSS Transactions on Power Electronics and Applications*. He was elected the President of CPSS in November 2021. Since 2013, he has been the Vice Chair of the Chinese National Steering Committee for College Electric Power Engineering Programs.

Zeng Liu (Member, IEEE) received the B.S. degree from Hunan University, Changsha, China, and the M.S. and Ph.D. degrees from Xi'an Jiaotong University (XJTU), Xi'an, China, in 2006, 2009, and 2013, respectively, all in electrical engineering.

He then joined XJTU as a Faculty Member in electrical engineering, where he is currently an Associate Professor. From 2015 to 2017, he was with the Center for Power Electronics Systems, Virginia Polytechnic Institute and State University, Blacksburg, VA, USA, as a Visiting Scholar. His research interests include control of power systems with multiple converters for renewable energy and energy storage applications, and small-signal stability of power electronics systems.

Dr. Liu was the recipient of two Prize Paper Awards in the IEEE TRANSACTIONS ON POWER ELECTRONICS. He is an Associate Editor for the IEEE OPEN JOURNAL OF POWER ELECTRONICS and on the Editorial Board for the *Energies*, and was the Secretary-General for 2019 IEEE 10th International Symposium on Power Electronics for Distributed Generation Systems and 2020 The 4th International Conference on HVDC.

Zhaoqi Song received the B.S. degree in electrical engineering in 2020 from Xi'an Jiaotong University, Xi'an, China, where he is currently working toward the M.S. degree in electrical engineering with the School of Electrical Engineering.

His research focuses on the control grid-interlinking converter.